Microenvironmental Constraint on δ^{13}C Depletion: Garudamangalam Sandstone, Cauvery Basin, India

Nivedita Chakraborty[a], Subir Sarkar[b*], Anudeb Mandal[c], Sunipa Mandal[b], Adam Bumby[d]

[a] *Department of Geology, K.J.R Govt. General Degree College, Bankura-722143,India*
[b] *Department of Geological Sciences, Jadavpur University, Kolkata-700032, India*
[c] *Department of Geology, Presidency University,Kolkata-700073,India*
[d] *Department of Geology, University of Pretoria, Pretoria-0002, S.A*

∗ Corresponding author Email: jugeoss@gmail.com

Abstract

Within the hydrocarbon-producing Cretaceous marine Uttatur Group, Cauvery Basin, India, the Garudamangalam Sandstone Formation is at top of a TST-HST transit. The δ^{13}C value is expectedly depleted within the calcareous Garudamangalam Sandstone, which is the top most unit of the Uttatur Group, overlying the Karai Shale. The calcareous sandstone was deposited in a coastal setting around a shore-parallel river mouth bar. Instances of excessive depletion of δ^{13}C up to -44.5‰ in the carbonate cement is suggestive of methane generation and its subsequent sequestration. The common occurrence of early diagenetic pyrite in these rocks testifies to the proliferation of sulfate-reducing bacteria and is suggestive of methane generation beneath the sulfate reduction zone. Upward-moving diffusive methane was possibly consumed by methanotrophs at the base of the sulfate-reduction zone. Abundant fabric-selective carbonate cement corroborates microbially-controlled anaerobic oxidation of methane. The presumed high rate of nutrient supply, abundance of vegetative material and moderately high organic carbon content in sediments (av. 1.6%), support this contention. All the samples which have the greatest δ^{13}C depletion are characterized by enriched organic carbon and are derived from a tidal inlet-mouth facies, and selectively from mud drapes on cross-bedding in tidal strata. Calcarenite at the

base of the same cross-strata are invariably much less depleted in δC^{13}. This range of relationships indicates the transport of methanotrophs that settled on foreset beds mostly as tides slackened under the broader control of neap-spring cycles.

Keywords: $\delta^{13}C$ Depletion, Methane, Methanotrophs transportation, Tidal slackening, Garudamangalam Sandstone

1. Introduction

An unusual negative excursion of $\delta^{13}C$ in calcite values approaching -50‰ is commonly correlated with methane sequestration (Claypool and Kaplan, 1974). The topic gains importance in the view of recent trend of ~1% yr^{-1} increase in atmospheric methane (Reeburgh, 2007 and references therein). Reeburgh (2007) made a review of earlier work on the natural processes of methanogenesis and methane oxidation. This paper focuses upon environmental constraints on spatial variation of $\delta^{13}C$, locally depleted to an extraordinary extent (-44.5‰) in the Cretaceous Garudamangalam Sandstone (GS), Trichinopoly, India (Fig. 1). It presents evidence for reworking of methanotrophs, originally invoked by Pohlman et al. (2013). It brings to light a selective environmental constraint on spatial variation of $\delta^{13}C$, which decreased values to about -50‰

Calcite precipitated inorganically from sea water yields $\delta^{13}C$ -2 to +2‰ PDB (Rollinson, 1993), while $\delta^{13}C$ values from organic carbon are much lower, at ~ -25‰ (Irwin et al., 1977; Rollinson, 1993). Methane $\delta^{13}C$ values are far more depleted; < -50‰ when biogenic, and lower when abiotic (Claypool and Kaplan, 1974; Henderson, 2004; Reeburgh, 2007). Whether
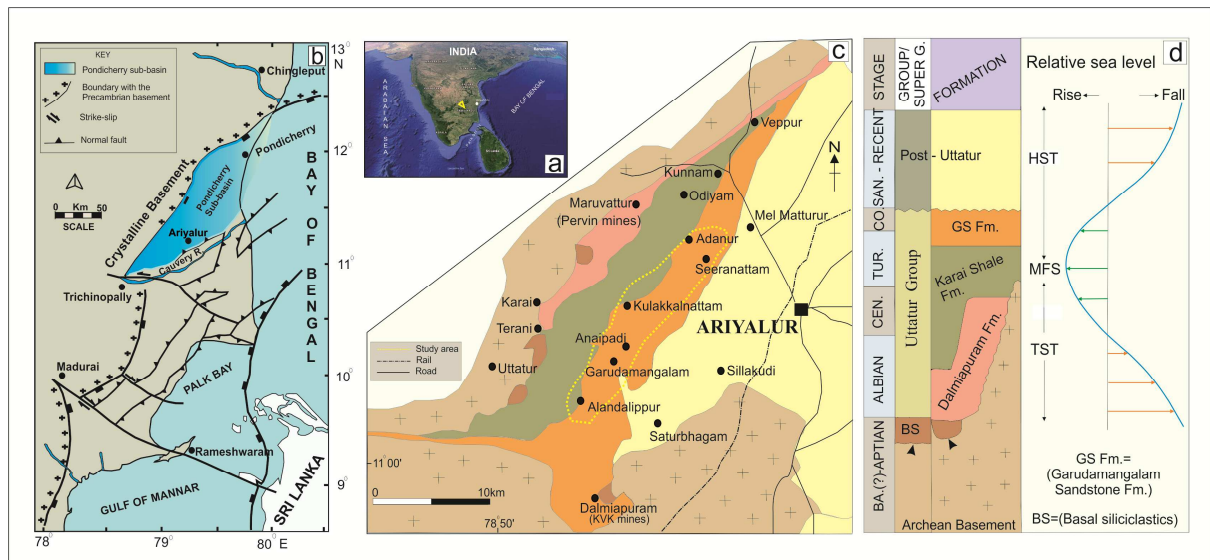
Fig.1. Part of Indian Map, the yellow arrow pointing the study area (a). The structural definition of Cauvery basin (b). Geological map showing spatial distribution of the Cretaceous Basal Siliciclastics and the three formations of the Uttatur Group (c). Stratigraphic context of the Uttatur Group (not to scale). The inferred relative sea level curve for the Uttatur Group (on further right) (d).

biogenic or abiotic, ^{12}C is preferentially lost upon oxidation, and hence the residual methane turns heavier.

Sarkar et al. (2014) proposed a shore-parallel deltaic mouth-bar palaeogeography during deposition of the GS, which may have significance in this regard, especially if the methane is biogenic. Bange et al. (1994) identified the coastal zone as source of ~75% global oceanic methane emission to the atmosphere. Supersaturation of methane in coastal waters readily arises because of the addition of organic matter, including vegetative organic matter especially rich in C^{12}, from land (Cynar and Yayanos, 1992; Ward, 1992). Additionally, the high rate of nutrient supply in a deltaic environment induces high rates of in-situ biogenic production and further boosts methane generation. Faecal pellets which are extraordinarily rich in methane are abundant in such an environment (Turner, 2002; Wilson and Schieber, 2015). Stagnant water in a back-barrier palaeoenvironment such as that associated with the GS would have caused further migration of the sulphate-methane transition to quite a shallow depth. Abundance of early diagenetic pyrite in almost all the facies comprising the GS (Sarkar et al., 2014) is consistent with the likely proliferation of sulphate-reducing bacteria favouring methanogenesis and methanotrophy. The broad frame of its shore-parallel deltaic bar palaeogegraphy (Sarkar et al., 2014; Fig. 2) explains the distinctiveness of the isotopic character of the GS. The organic carbon content of different facies within this formation is variable ranging from 0.66 to 4.90.

2.   Geological context

The Upper Cretaceous Garudamangalam Sandstone Formation is the top-most formation of the Uttatur Group within the hydrocarbon (oil and natural gas) producing Cauvery rift basin, SE India (Sarkar et al., 2014; Fig. 1a,b,c). Atop the fluvial Basal Siliciclastic Formation
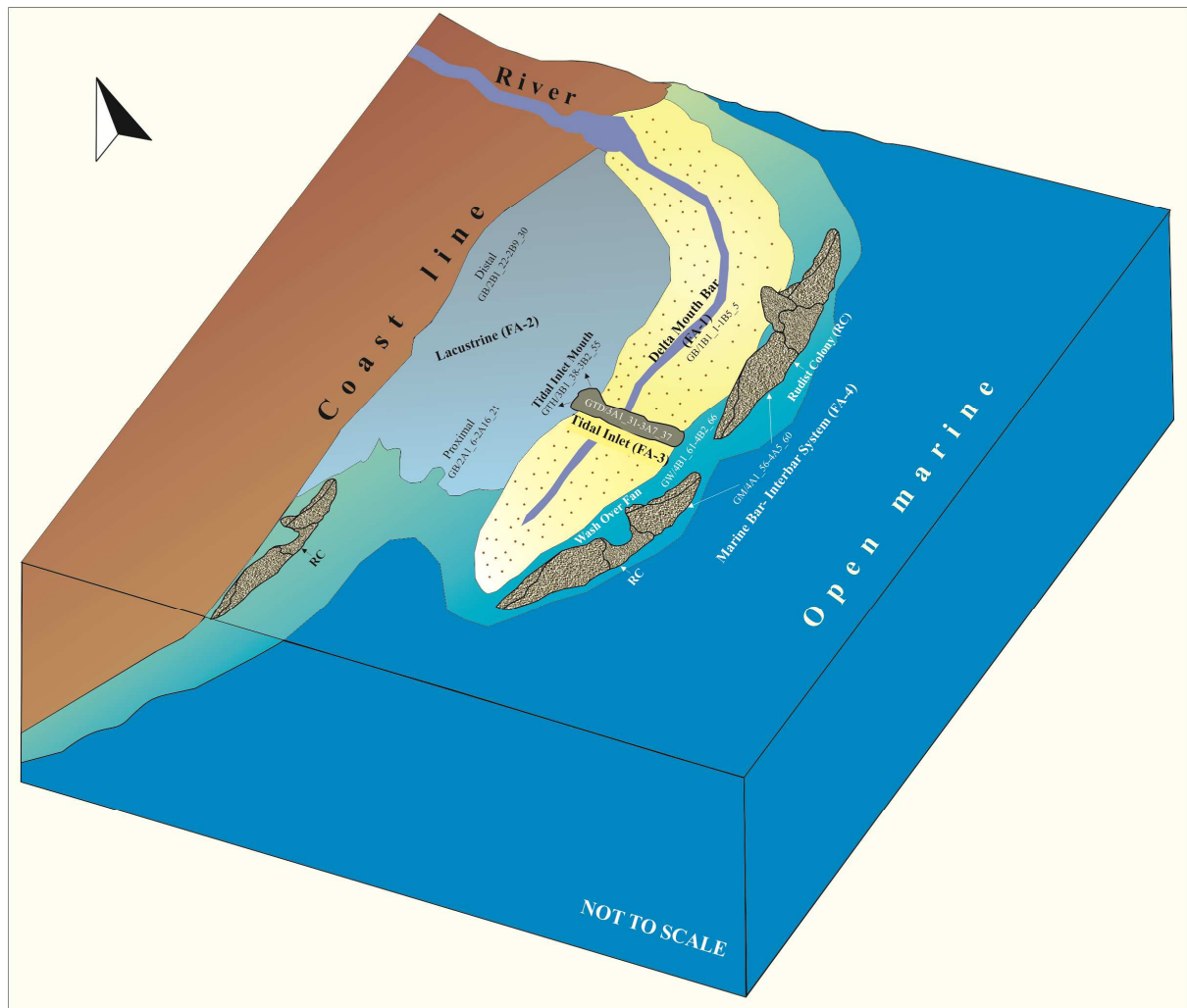
Fig.2. Model for palaeogeography of deposition of the GS (not to scale; modified after Sarkar et al., 2014). The samples collected from the different palaeogeographic sectors are mentioned accordingly in the number ranges.

(Chakraborty et al., 2017), limestones of the open marine Dalmiapuram Formation grade upward into the Karai Shale Formation, reflecting further expansion and deepening of the depositional basin (Nagendra et al., 2013, 2017; Watkinson et al., 2007; Fig.1d). The limestone-shale transition constitutes a transgressive systems tract (TST) up to the level of the maximum flooding surface (Banerjee et al., 2016; Nagendra et al., 2011, 2017). Further above, the coarsening-upward part of the Karai Shale grades into the GS constituting a highstand systems tract (HST) before terminating against an unconformity (Tewari et al., 1996; Sarkar et al., 2014; Fig.1d). The *ca.* 490m-thick sandstones of the Garudamangalam Formation (Sundaram et al., 2001), are locally exposed along a NE-SW trending outcrop belt, in the vicininty of Ariyalur, Trichinopoly (Figure 1c). All these strata were deposited within the onshore palaeoenvironment of the Cauvery basin. These GS strata are considered as co-eval to the offshore Kudavasal Formation (Govindan et al., 2000). The GS is a mixed siliciclastic-carbonate formation, abundant in marine macrofossils (ammonites, bivalves including encrusting oysters, abundant gastropod shells, and brachiopods); planktonic foraminifera and calcareous nannoplanktons as well as trace fossils like *Skolithos* and *Cruziana* (Ayyasami and Banerji, 1984; Govindan et al., 1996; Hart et al., 1996; Nagendra et al., 2010). Sarkar et al. (2014) interpreted a river mouth bar palaeogeography for this formation in a shallow marginal marine setting.

3. Facies

The river mouth bar-related palaeogeography of the GS comprises four facies associations, viz. river-dominated deltaic bar, restricted bay or lagoon, tidal inlet and marine. Each of these four facies associations are subdivided into two individual facies and one of the

Table 1. Facies constituents of the Garudamangalam Sandstone Formation (GS).

Facies Association	Facies	Description	Interpretation
FA 1. Medium-coarse grained sandstone, sometimes granular and with few skeletal fragments, remarkably poor sorting,typically characterized by trough cross-strata; Trace fossil: Glossofungitesassociation, Thalassinoides, oblique Ophimorpha, suspected Arenicolites in 1A and sponge -liomorpha in 1B	1A	Entirely siliciclastic, siliciclastic mud fills interstitial spaces among framework grains, recrystallization of mud matrix along the margin of framework; distinctly coarser than the other, cross-sets thickness up to ~25cm, quartz, feldspar and biotite comprise the framework population, decomposed feldspar grains preferably along cleavage planes, bleached biotite grains preferably along their margins; wood fragments with lengths of up to 81cm.	River-dominated deltaic bar
	1B	Flat bases convex-up geometry, internally trough cross stratified and sigmoidal cross-strata at the flanks, calcareous sandstone beds(~1m) alternating with planar or ripple-laminated siltstonesor silty shales(~6cm), the comparatively finer grained, interstitial spaces filled by dirty calcite spar, sand crystals present, sigmoidal cross-stratas(~15cm) oriented at high angles to the trough cross-strata(set thickness ~12cm, poorly sorted.	
FA 2. Very fine-grained sandstone and siltstone with carbonate mud in groundmass, very limited burrowing activities	2A	Internally characterized by trough cosets (individual cross-sets thickness up to 11cm), wood fragments (max 10cm) present, local growth convex-up organic patches of indeterminate origin and irregular patches of thick-cemented shells of sedentary bivalves, moderately sorted, usually fresh feldspar grains replaced by carbonates along cleavage planes and quartz grains nibbled at their margins, specks of glauconite, opaque grains of pyrite scattered within the groundmass.	Restricted bay or lagoon

Facies Association	Facies			Description	Interpretation
	2B			Reddish well-sorted siltstone with skeletal grains and silt-sized siliciclastic grains floating within carbonate mud, minuscule red algae growth, micritic rims are present on many shells, abun-dance of glauconite, is present in relatively greater than in facies 2A, small specks of pyrite.	
FA 3. Moderately-sorted sandstone alternating with heterolithic unit with contrasting framework com-positions, viz. siliciclastic and calcareous, monospecific ichnofacies assembledge of Glossifungites including Planolites, Bergaueria and Gyrolithes	3A			Cross-stratified, planar at places and troughs elsewhere. Dune-like bedforms (average height 42cm), substantial shell concentration at the toe of these bedforms, well-defined mud drapes, framework elements often found detached from each other and floating within the carbonate groundmass made of blocky calcite crystals, sand grains present, carbonate crystals are generally dirty in appearance, pyrite crystals present, glauconite grains, both fresh and oxidized, locally present.	Tidal inlet
	3B	3B1		Well sorted, thinner bodies not exceeding 6-7 cm, internally it is cross-stratified or planar-laminated, but it may also be massive, frame-work grains here also float within the car-bonate groundmass made of blocky calcite, sand crystals present, dirty carbonate crystals contain relict grains, quartz and feldspar grains have nibbled margins, the feldspar grains are preferably replaced by carbonates along cleavage planes, both fresh and oxidized glauconite pellets are present.	
		3B2		Dominance of carbonate skeletal material concentrated preferably along bases of foresets (av. thickness 4cm), characteristically draped by reddish mud; vertical burrows (diameter ~3cm, length 15cm) with fuzzy boundaries, burrow-fills are characterized by sand-mud alternations with almost absence of shell, feldspar grains are characteristically fresh in nature, quartz and feldspar grains are nibbled and replaced by carbonate along their margins, drusy growth present only within some mouldic pores	

Facies Association	Facies	Description	Interpretation
FA 4, Well-sorted cross stratified calcareous sandstone, Thalassinoides are and sponge borings are abundant	4A	Medium-grained, moderate-to well-sorted, trough cross stratified sandstone (up to 10cm thick), local intense bioturbation and small patchy bioherms of rudists bivalves, numerous polygonal cracks as well as minute borings, small blebs of glauconite are present in fairly high frequency, framework population in this facies includes quartz, feldspar and numerous skeletal fossils, feldspars are generally fresh, interstitial spaces between framework elements are filled by clear blocky calcite spar.	Marine
	4B	Heterolithic facies, found only in small patches not exceeding 3m in lateral extent and 1.5m in thickness, presumably erosional, concave-up base and a slightly convex-up top, internally being characterized by repeated alternations between thicker shell-rich beds and thinner internally massive reddish mud beds, shell bands have a somewhat irregular geometry because of lateral pinching and swelling, load casts present at the base of shelly beds, locally normal grading, authigenic glauconite globules are common, minute crystals of authigenic pyrite, interstitial spaces between framework grains are filled by blocky calcite shells commonly retain their primary fabric.	

facies (3B) into two sub-facies (Fig. 2). Facies and sub-facies are distinguished on the basis of lithology and structure with the prime objective to understand their sedimentatary dynamics. Facies associations, on the other hand, highlight the palaeogeography of deposition. Table 1 presents necessary characteristic of facies constituents of the Garudamangalam Sandstone Formation. For further details the reader is referred to Sarkar et al., (2014). The palaeogeographic model in Sarkar et al. (2014) has been utilized here with some modifications to represent palaeogeographic information about the samples used for the present purpose (Fig.2).

4. Analytical methods

4.1. Isotope Analysis

Analyses were conducted at various stratigraphic levels of the Dalmiapuram (limestone) Formation, Karai Shale Formation (excluding the extraneous calcarenite facies; Chakraborty et al., 2013) and Garudamangalam Sandstone Formation (all facies/subfacies). For carbon and oxygen stable isotope analysis, powdered samples of carbonate were prepared to react with ~100% phosphoric acid at 80°C using GEO 20-20 stable isotope ratio mass spectrometer (CFIRMS) at the National Stable Isotope Facility of IIT, Kharagpur and Kiel IV Carbonate Device connected to the MAT 253 mass spectrometer in dual inlet mode at IISER, Kolkata. All the values are reported in per mil (‰) relative to the VPDB standard (w.r.t NBS-18, 19 carbonate, BDH (Univ. Coll. London) and Z-Carrara (PRL/Cambridge Univ.)). Experimental precision of ±0.1 ‰ and ±0.05‰ were maintained respectively.

4.2. Carbon Content and Character

Inorganic and organic carbon contents of samples from different facies at different level within the Garudamangalam Sandstone Formation were measured. The analysis was carried out in the Department of Geology, Delhi University, using SHIMADZU total organic carbon analyzer (TOC-L$_{CPH/CPN}$) and solid sample module (SSM-5000A), which adopts the 680℃ combustion catalytic oxidation method. While providing an ultra-wide range of 4 μg/L to 30,000 μg/L, it boasts a detection limit of 4 μg/L through coordination with non-dispersed infrared (NDIR). The solid sample module (SSM) was used to oxidize powdered solid samples, which were then directed to the NDIR detector within TOC-L instrument for analysis. The solid samples were heated at 900℃ and 200℃ for TC and IC evaluation, respectively within the solid sample module.

Diamond polished sections of tidal mud laminae were scanned to check kerogen composition by Raman Spectroscopy with a Renishaw inVia Raman Microscope illumination at 514nm-785nm (with beam diameter ~1μm and focus ener gy ~15-18mW) attached with a Philips SPC1036NC webcam at GSI, Kolkata Head Quarters, India. The spectral range of the spectrometer is c. 1200-2400cm^{-1} . Raman spectra were compared with reference spectra from RRUFF Database (Downs, 2006), and spectra from published literature (e.g. Schopf and Kudryavtsev, 2005).

5. Results

The results of carbon and oxygen isotope analyses are presented in Table. 2. The δ^{13}C values in the TST section composed of the Dalmiapuram Limestone and the lower part of the Karai Shale are close to open marine values (Fig.3). In the HST section, including the GS, they
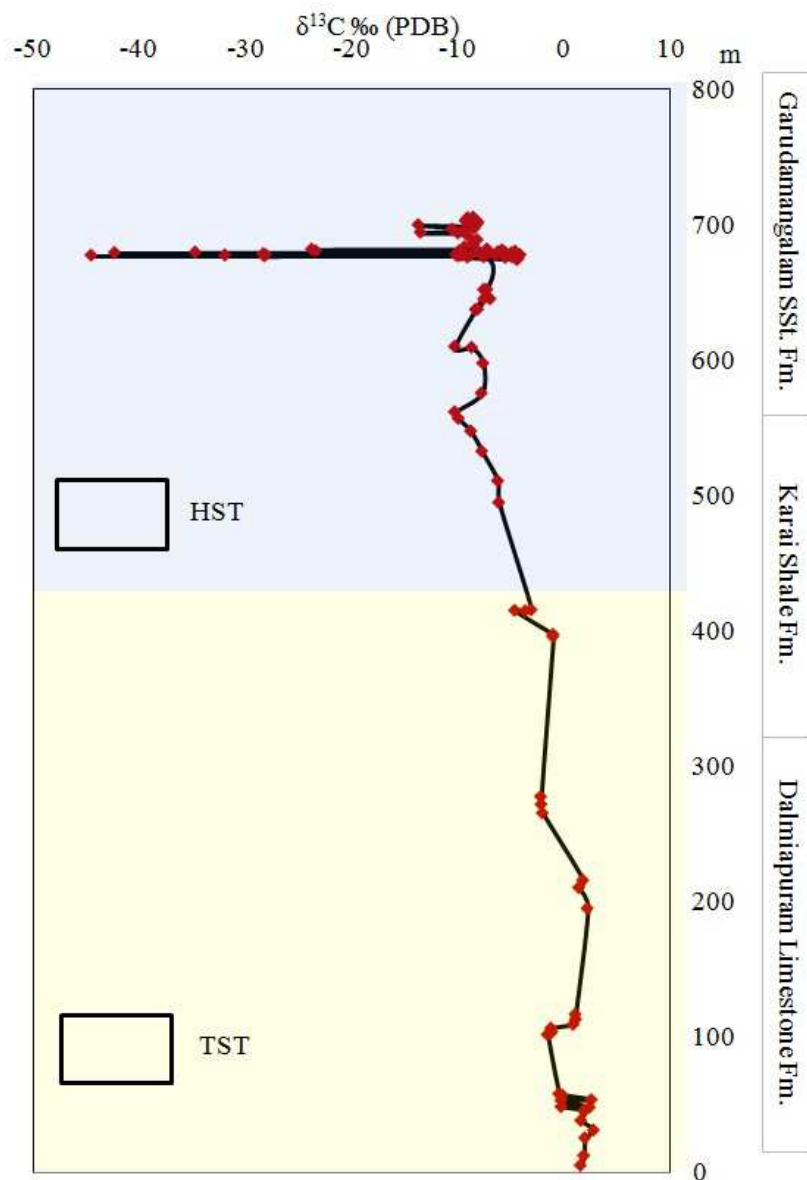
Fig.3. $\delta^{13}C$ stratigraphy within the Uttatur Group divided in TST and HST. There is a negative swing within the HST with respect to the TST. Note unusually long negative excursion at a mid-level of the Garudamangalam Sandstone (GS).

Table 2. Carbon and oxygen isotope composition of Garudamangalam Sandstone Formation

Sample No.	$\delta^{13}C$‰ (VPDB)	$\delta^{18}O$‰ (VPDB)
GB/1B1_1	-4.3	-6.8
GB/1B2_2	-4.4	-6.9
GB/1B3_3	-4.3	-3.7
GB/1B4_4	-4.1	-3.5
GB/1B5_5	-4.6	-4.3
GL/2A1_6	-13.7	-5.7
GL/2A2_7	-8.4	-5.9
GL/2A3_8	-10.5	-9.0
GL/2A4_9	-9.4	-3.8
GL/2A5_10	-13.5	-3.8
GL/2A6_11	-10.0	-3.4
GL/2A7_12	-8.8	-7.6
GL/2A8_13	-8.1	-3.7
GL/2A9_14	-8.5	-3.6
GL/2A10_15	-9.3	-2.8
GL/2A11_16	-9.8	-7.3
GL/2A12_17	-7.1	-8.2
GL/2A13_18	-10.1	-3.8
GL/2A14_19	-9.6	-3.9
GL/2A15_20	-9.9	-4.0
GL/2A16_21	-9.1	-3.7
GLD/2B1_22	-8.5	-7.4
GLD/2B2_23	-9.0	-7.5
GLD/2B3_24	-8.4	-7.9
GLD/2B4_25	-8.4	-7.9
GLD/2B5_26	-9.3	-3.6
GLD/2B6_27	-8.5	-3.9
GLD/2B7_28	-8.1	-8.4
GLD/2B8_29	-8.1	-5.0
GLD/2B9_30	-8.5	-8.2
GTD/3A1_31	-5.8	-3.1
GTD/3A2_32	-5.5	-3.3
GTD/3A3_33	-4.9	-6.5
GTD/3A4_34	-4.9	-6.2
GTD/3A5_35	-5.5	-3.7
GTD/3A6_36	-7.5	-5.6
GTD/3A7_37	-5.6	-4.9
GTH/3B11_38	-44.5	-6.8
GTH/3B21_39	-8.7	-4.3

Sample No.	$\delta^{13}C‰$ (VPDB)	$\delta^{18}O‰$ (VPDB)
GTH/3B12_40	-31.9	-6.9
GTH/3B22_41	-6.4	-5.9
GTH/3B13_42	-28.1	-8.4
GTH/3B23_43	-5.0	-7.0
GTH/3B14_44	-42.3	-5.8
GTH/3B24_45	-7.5	-5.4
GTH/3B15_46	-34.7	-7.5
GTH/3B25_47	-6.2	-5.1
GTH/3B16_48	-23.7	-5.4
GTH/3B26_49	-7.2	-3.6
GTH/3B17_50	-23.4	-5.1
GTH/3B27_51	-8.1	-4.9
GTH/3B18_52	-28.3	-5.0
GTH/3B28_53	-7.2	-8.2
GTH/3B19_54	-28.2	-5.2
GTH/3B29_55	-7.6	-7.3
GM/4A1_56	-10.3	-7.6
GM/4A2_57	-8.7	-7.6
GM/4A3_58	-7.6	-3.4
GM/4A4_59	-7.7	-3.5
GM/4A5_60	-7.0	-8.2
GW/4B1_61	-8.3	-4.0
GW/4B2_62	-8.1	-3.7
GW/4B1_63	-7.5	-7.4
GW/4B2_64	-6.9	-8.0
GW/4B1_65	-7.5	-7.0
GW/4B2_66	-7.2	-7.6

Table 3. Organic carbon (OC), Inorganic carbon (IC) and Total Organic Carbon (TOC) contents within Garudamangalam Sandstone Formation.

Sample no	Total Carbon (%)	Inorganic Carbon (%)	Total Organic Carbon (%)
GB/1B1_1	0.66	0.00	0.66
GB/1B2_2	4.22	2.39	1.83
GB/2A1_6	3.85	2.37	1.50
GB/2A2_7	6.11	3.84	2.30
GB/2B1_22	4.48	3.36	1.12
GB/2B2_23	6.04	4.48	1.56
GTD/3A1_31	2.03	1.16	0.90
GTD/3A2_32	3.14	2.02	1.11
GTH/3B11_38	5.14	4.22	0.92
GTH/3B21_39	3.11	2.23	0.88
GTH/3B12_40	5.95	3.08	2.90
GTH/3B22_41	3.87	1.98	1.90
GM/4A1_56	5.76	4.55	1.21
GM/4A2_57	10.03	5.13	4.90
GW/4B1_61	3.32	2.18	1.14
GW/4B2_62	2.95	2.09	0.90
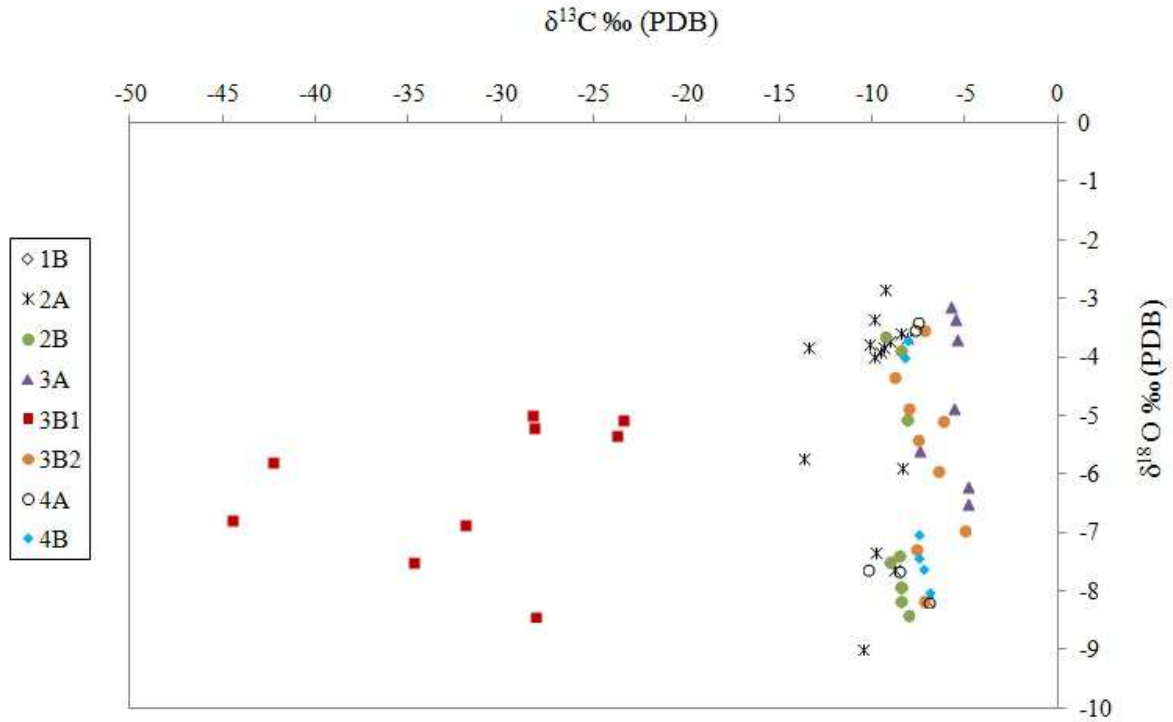
Fig.4. δ^{13}C vs. δ^{18}O plot for different facies constituting the GS. Separate symbols have been used for different facies that correspond to their respective palaeogeographies indicated in Fig. 2. The red solid square symbol stands for the mudstone sub-facies (3B1) and orange solid circles for the calcarenite sub-facies (3B2) within tidal inlet-mouth heterolithic facies (3B). Note that the plots for the facies 3B are clustered wide apart depending on lithology.
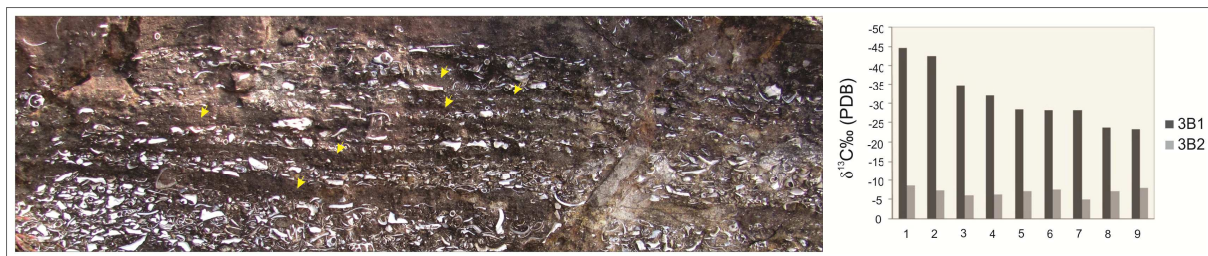
Fig.5. Calcarenite foresets with mud drapes, indicated by yellow arrows, within tidal inlet-mouth heterolithic facies (3B) (on left). The $\delta^{13}C$ of the numbered lamina couplets (3B1=mud drapes; 3B2= calcareous skeletal material) are displayed in a bar diagramme (on right); the grey bars are for the calcarenite and the dark bars are for the mudstone lithology. Note that $\delta^{13}C$ values are considerably more depleted in mudstone than the calcarenite subjacent to them. Further note the upward thinning of the mudstone laminae, possibly in response to tidal neap-spring cycle and lesser depletion of the $\delta^{13}C$ values.

take a negative excursion. However, in nine cases the excursion is significantly lower (-44.5 to -23.4‰) in comparison to others (Fig.3). In a δ^{13}C vs. δ^{18}O plot these values appear distinctly aberrant (Fig.4). It is significant that all nine of these anomalous data came from a single sub-facies (3B1) representing the reddish mudstone on top of some tidal foresets. Even more significant is that their calcarenite counterparts (3B2) at the base of the same foresets have contrastingly heavier values (Fig.5). The δ^{13}C values of samples from other facies vary from -4.1 to -13.7 (Table.1,2).

The presence of a moderate amount of inorganic carbon (max. 4.55 wt.%) in all but one of the facies/subfacies studied is consistent with the general calcareous nature of the rocks in the GS Formation (Table. 3). All of the facies associations constituting the GS are rich in carbonate. Organic carbon content is somewhat elevated, mostly >1%, but does not display any apparent correlation with either inorganic carbon content, or with δ^{13}C (Table. 3). The presence of organic carbon in tidal mud laminae (3B1) has been reconfirmed by Raman analysis (Fig. 6).
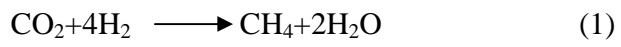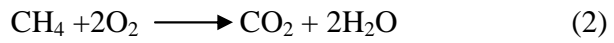
6. Discussion

6.1. Methane production and consumption

General depletion of δ^{13}C in the HST compared to the TST within the Uttatur Group is presumably because of the mixing of meteoric water rich in ^{12}C. However, δ^{13}C as low as -44.5‰ in sub-facies 3B1 of the tidal inlet association cannot be explained without the involvement of methane (Katz, 2011; Reeburgh, 2007; Whiticar,1999), while the values of the other associated facies within the same association are less negative. Organic matter decomposition beneath the sulphate reduction zone is typically through biogenic methanogenesis (eqn.1, Box; Fig.7). Had methane been so generated in the GS it would have diffused upward and then been oxidized
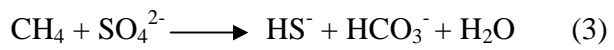
Box

Biogenic Methanogenesis

$$CO_2 + 4H_2 \longrightarrow CH_4 + 2H_2O \qquad (1)$$

Aerobic Oxidation of Methane

$$CH_4 + 2O_2 \longrightarrow CO_2 + 2H_2O \qquad (2)$$

Anaerobic Oxidation of Methane

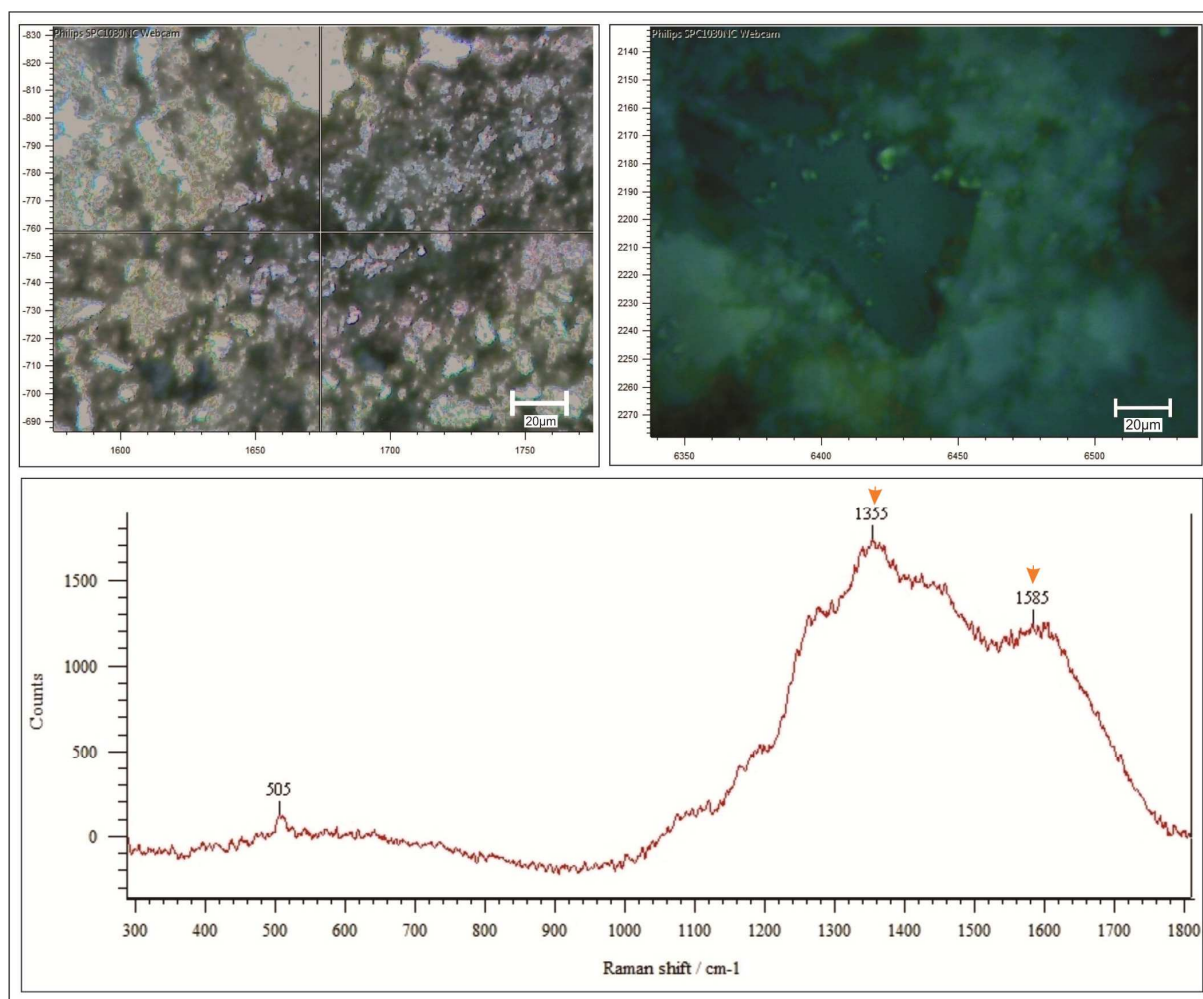$$CH_4 + SO_4^{2-} \longrightarrow HS^- + HCO_3^- + H_2O \qquad (3)$$

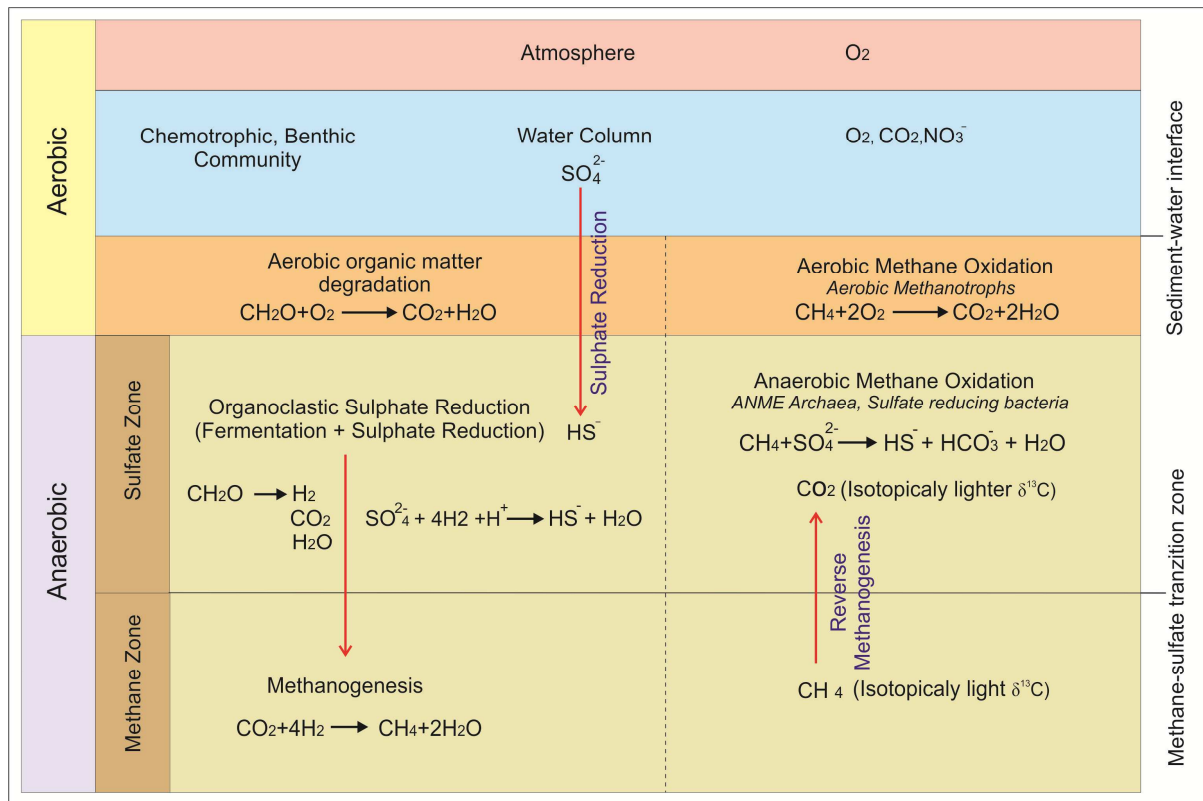**Fig.6.** Organic carbon showing characteristic peaks under Raman Spectroscopy.

Fig.7. Flow-chart showing microbialy mediated carbon transformation, pathways of methane production (methanogenesis) and consumption (reverse methanogenesis) under aeorobic and anaerobic conditions.

within the sediment to a variable extent before emission into the water column and atmosphere. This oxidation with preference for ^{12}C leaves the residual methane heavier than what it had been earlier, by the relative concentration of ^{13}C. It accounts for the δ^{13}C values close to, though heavier than -50‰, as obtained from the GS. Aerobic oxidation of methane within sediment is inordinately slow and results in an increase in acidity, favoring carbonate dissolution. (Lovely and Klug, 1986, Reeburgh, 2007; eqn.2, Box; Fig.7). In the absence of evidence for large-scale carbonate dissolution, this mechanism seems unlikely in the present case. Instead, large-scale fabric-selective carbonate precipitation in almost all the GS facies (Sarkar et al., 2014) supports anaerobic oxidation of methane (AOM) (eqn.3, Box; Fig.7) and the consensus is that the anaerobic process is considerably more effective at oxidation (Reeburgh, 2007 and references there in). AOM is essentially microbially-mediated, and microbiota like Archaea and sulphate reducing bacteria presumably oxidized the methane generated within the GS (cf. Pohlman et al., 2013; Reitner et al., 2005). Prolific growth of sulfate-reducing bacteria is suggested by the abundance of disseminated pyrite within the majority of facies constituting the GS (Fig. 8). Immediately above the sulfate-methane transition, in the scarcity of sulfate, the sulfate-reducing bacteria had to partition their survival strategy between reduction of whatever little sulfate was still available and oxidation of the upward diffusing methane (Reeburgh, 2007).

6.2. Palaeogeographic significance

Organic carbon content in excess of 1% satisfies the prime prerequisite for biogenic methane generation (Clayton, 1992; Rice, 1993). It can be presumed that the supply of organic matter was at a rate in excess of its rate of oxidative degradation. The common occurrence of a clotted texture within the carbonate matrix in the back-barrier deposits of the GS suggests

Fig.8. Disseminated pyrites under cross-nichols from the facies 3B (marked by yellow arrow head).

enrichment in faecal pellets (Sarkar et al., 2014) that constitute a rich source of biogenic methane. The rate of nutrient supply at the delta mouth is considered to have been adequate to sustain a good population of local biota. The inlet mouth sub-facies (3B1) that is associated with all the unusually depleted $\delta^{13}C$ values is the one that, within the broad deltaic palaeogeographic frame of deposition, possibly received maximum nutrient supply both from land and sea. Being enriched with plenty of organic matter, including C^{12}-rich vegetative matter, this particular environment had all the ingredients on which a vast population of local biota could thrive. The high rate of organic matter supply to the site could have been quite favorable for methane generation, but conceivably also for methanotrophy. Excessive amounts of organic matter at the base of sulphate reduction zone would leave less oxygen after degradation and fewer options for sulphate-reducing bacteria. This results in switch over of the mechanism from sulphate reduction to methanotrophy as an alternative strategy (Katz, 2001). Withdrawal of more favored electron acceptors like Fe^{+2} or SO_4^{-2} in pyrite beforehand made the early diagenetic system especially fit for methanotrophy (Reeburgh, 2007). Also presence of excessive organic matter could have moved the methane-sulfate transition to a shallower level within the reach of erosion, particularly on occasions of enhanced energy input, such as storms. Thus the methanotrophs may be scooped up, transported and deposited elsewhere.

The nine pairs of samples collected from this particular tidal inlet-mouth palaeoenvironment disclose a startling pattern in $\delta^{13}C$ variations (Fig. 5). Every mud drape on top of the foresets has $\delta^{13}C$ distinctly more depleted compared to its immediately underlying calcarenite counterpart. The mode of sediment transport evidently controlled the variation. The physical redistribution of methanotrophs in tidal water, similar to that suggested by Pohlman et al. (2013), seems to be the appropriate explanation for this observation. The methanotrophs

settled preferably with mud during tidal slackening. It can be presumed that tidal waxing and waning was accentuated and manifest in deposits at the mouth of the constricted tidal inlets. All the mud drapes in this microenvironment are not equally depleted in $\delta^{13}C$ possibly because of the temporally variable extent of tidal slackening. Tidal neap-spring cycles conceivably had an important control on this factor. The wide-ranging variation in $\delta^{13}C$ values obtained from the GS, in general, possibly depended on the variable rate of accumulation of methanotroph bodies in various subenvironments that comprised the deltaic palaeogeography.

7. Conclusion

The negative excursion of $\delta^{13}C$ values within the sandstones of the Upper Cretaceous Garudamangalam Formation, Ariyallur District, India could be expected as it forms the terminal part of a HST. Unusual depletions of up to -44.5‰ however, call for methanogenesis below the sulphate reduction zone. The methane that diffused upwards and underwent anaerobic oxidation became heavier through the concentration of $\delta^{13}C$ than its original isotopic concentration. All of the unusually depleted $\delta^{13}C$ values come from a particular environmental sector, at the landward mouth of tidal inlets that had cut across the shore-parallel deltaic bar. Furthermore, $\delta^{13}C$ depletions are restricted only to the mudstone lithology. Although not all the mudstones of this environmental sector are similarly depleted, they are always distinctly more depleted than the calcarenites they are coupled with in the tidal foresets. The transport of methanotrophs in suspension can only explain such lithological control on concentration of the depleted $\delta^{13}C$ values. Enrichment of sediment with reworked methanotrophs and consequently the extent of the $\delta^{13}C$ depletion in sediments depended largely on the extent of tide slackening in the broad frame of neap-spring cycles.

Acknowledgements

References

Ayyasami, K., Banerji, R.K., 1984. Cenomanian-Turonian transition in the Cretaceous of southern India. Bulletin of the Geological Society of Denmark. 33, 21-30.

Banerjee, S., Bansal, U., Pande, K., Meena, S.S., 2016. Compositional variability of glauconites within the Upper Cretaceous Karai Shale Formation, Cauvery Basin, India: implications for evaluation of stratigraphic condensation. Sedimentary Geology. 331, 12-29.

Bange, H.W., Bartell, U.H., Rapsomanikis, S. Andreae, M.O., 1994. Methane in the Baltic and North Seas and a reassessment of the marine emissions of methane. Global Biogeochemical Cycles. 8, 465- 480.

Chakraborty, N., 2013. Indigenous siliciclastic and extraneous polygenetic carbonate beds in the Albian-Turonian Karai Shale, Ariyalur, India. In: International conference (IGCP-608)

Cretaceous Ecosystem and Their Response to Palaeoenvironmental Changes in Asia and West Pacific, Abstract Volume, p.5.

Chakraborty, N., Sarkar, S., Mandal, A., Mejiama, W., Tawfik, H. A., Nagendra, R., Bose, P.K. Eriksson, P. G., 2017. Physico-chemical Characteristics of the Barremian-Aptian Siliciclastic Rocks in the Pondicherry Embryonic Rift Sub-basin, India, in: Mazumdar, R., (Ed.), Sediment provenance: Influences on Compositional Change from Source to Sink. Elsevier, Ch. 6, pp. 85-121. http://dx.doi.org/10.1016/B978-0-12-803386-9.00006-X.

Claypool, G. E., Kaplan, I. R., 1974. The origin and distribution of methane in marine sediments, in: Kaplan, I. R., (Ed.), Natural Gases in Marine Sediments. Plenum Press, New York, pp. 99-139.

Clayton, C, 1992. Source volumetrics of biogenic gas generation, in: Vially, R., (Ed.), Bacterial gas: Paris, Edition Technip. pp. 191-204.Cynar, F. J., and Yayanos, A. A., 1992. The distribution of methane in the upper water of the southern California Bight. Journal of Geophysical Research. 97 (C7), 11269-11285.

Govindan, A., Ravindran, C. N. and Rangaraju, M. K., 1996. Cretaceous stratigraphy and planktonic foraminiferal zonation of Cauvery Basin, South India: Memoirs of the Geological Society of India. 37, 155-187.

Govindan, A., Ananthanarayanan, S., Vijayalakshmi, K.G., 2000. Cretaceous petroleum system in Cauvery basin, India, in: Govindan A (Ed.), Cretaceous Stratigraphy –An Update. Memoirs of the Geological Society of India 46, pp. 365–382.

Hart, M.B., Tewari, A.T., Watkinson, M.P., 1996. Wood borings from theTrichinopoly sandstone of the Cauvery Basin, South-East India, in: Pandey, J., Azmi, R.J., Bhandari, A. & Dave, A. (Eds.), Contributions XVth Indian Colloquium on Micropalaeontology and Stratigraphy, Dehra Dun, pp. 529–539.

Henderson, R. A, 2004. A Mid-Cretaceous Association of Shell Beds and Organic- rich Shale: Bivalve Exploitation of a Nutrient-Rich, Anoxic Sea-floor Environment. Paleos. 19, 156-169.

Irwin, H., Curtis, C., and Coleman, M., 1977. Isotopic evidence for source of diagenetic carbonates formed during burial of organic-rich sediments. Nature. 269, 209-213.

Katz, B. J., 2001. Lacustrine basin hydrocarbon exploration – current thoughts. Journal of Paleolimnology. 26, 161-179.

Katz, B. J., 2011. Microbial Processes and Natural Gas Accumulations. The Open Geology Journal. 5, 75-83.

Lovely, D. R., and Klug, M. J., 1986. Model for the distribution of sulfate reduction and methanogenesis in fresh water sediments. Geochimica et Cosmochimica Acta. 50, 11-18.

Nagendra, R., Patel, S.J., Deepankar, R., Reddy, A.N., 2010. Bathymetric significance of the ichno fossil assemblages of the Kulakkalnattam Sandstone, Ariyalur area, Cauvery Basin. Journal Geological Society of India. 76, 525-532.

Nagendra, R., Kamalak Kannan, B. V., Sen, G., Gilbert, H., Bakkiaraj, D., Reddy, A. N., and Jaiprakash, B. C., 2011. Sequence surfaces and paleobathymetric trends in Albian to Maastrichtian sediments of Ariyalur area, Cauvery Basin, India: Marine and Petroleum Geology. 28 (4), 895-905.

Nagendra, R., Sathiyamoorthy P., Pattanayak S., Reddy A. N., and Jaiprakash B. C., 2013. Stratigraphy and Paleobathymetric Interpretation of the Cretaceous Karai Shale Formation of Uttatur Group, TamilNadu, India. Stratigraphy and Geological Correlation. 21 (7), 675-688.

Nagendra, R., Reddy A. N., 2017. Major geologic events of the Cauvery Basin, India and their correlation with global signatures - A review. Journal of Palaeogeography. 6 (1), 69-83.

Pohlman, J. W., Riedel, M., Bauer, J. E., Canuel, E. A., Paull, C. K., Lapham, L., Grabowski K. S., Coffin, R. B. and Spence, G. D., 2013. Anaerobic methane oxidation in low-organic content methane seep sediments. Geochimica et Cosmochimica Acta. 108, 184–201.

Ramasamy, S. and Banerji, R.K. 1991. Geology, petrology and systematic stratigraphy of pre-Ariyalur sequence in Tiruchirapalli District, TamilNadu, India: Journal of the Geological Society of India. 37, 577–594.

Reeburgh, W. S., 2007. Oceanic methane biogeochemistry: Chemical Reviews. 107, 486–513.

Reitner, J., Peckmann, J., Blumenberg, M., Michaelis, W., Reimer, A., Thiel, V., 2005. Concretionary methane-seep carbonates and associated microbial communities in Black Sea sediments. Palaeogeography, Palaeoclimatology, Palaeoecology. 227, 18–30.

Rice, Dudley D. 1993. Biogenic gas: controls,habitats, and resource potential in in The future of energy gases, U.S. Geological Survey Professional Paper, 1570.

Rollinson, H.R., 1993. Using geochemical data: Evaluation, presentation, interpretation, (Ed.), Longman Group UK Ltd.

Sarkar, S., Chakraborty, N., Mandal, A., Banerjee, S., and Bose, P.K., 2014. Siliciclastic-carbonate mixing modes in the river-mouth bar palaeogeography of the Upper Cretaceous Garudamangalam Sandstone (Ariyalur, India). Journal of Palaeogeography. 3 (3), 233-256.

Sundaram, R. and Rao, P.S. 1986. Lithostratigraphy of Cretaceous and Palaeocene rocks of Tiruchirapalli District, Tamil Nadu, South India: Records of the Geological Survey of India. 115, 9–23.

Tewari, A., Hart, M. B., and Watkinson, M. P., 1996. A revised lithostratigraphical classification of the Cretaceous rocks of Trichinopoly District, Cauvery Basin, Southeast India, in: Pandey, J., Azmi, R. J., Bhandari, A., Dave, A., (Eds.), Contributions to XV Indian Colloquium on Micropaleontology and Stratigraphy. Dehra Dun: The K. D. Malaviya

Institute of Petroleum Exploration and the Wadia Institute of Himalayan Geology. pp. 789-800.

Turner, J.T., 2002. Zooplankton fecal pellets, marine snow and sinking phytoplankton blooms. Aquatic Microbial Ecology. 27, 57–102.

Ward, B. B., 1992. The subsurface methane maximum in the Southern California. Continental Shelf Research. 12(5/6), 735-752.

Watkinson, M. P., Hart, M. B. Joshi, A., 2007. Cretaceous tectono-stratigraphy and the development of the Cauvery Basin, South-east India. Petroleum Geoscience. 13 (2), 181-191.

Wilson, R. D., Schieber, J., 2015. Sedimentary Facies and Depositional Environment of the Middle Devonian Geneseo Formation of New York, USA. Journal of Sedimentary Research 85, 1393-1415.

Whiticar, M.J.,1999. Carbon and hydrogen isotope systematic of bacterial formation and oxidation of methane. Chemical Geology. 161, 291-314.

Highlights

- Methanotrophs settling on tidal slackening
- Methanogenesis
- Marked laterally variable degree of $\delta^{13}C$ depletion
- Tidal inlet mouths across shore-parallel delta favoured